JGR Atmospheres

RESEARCH ARTICLE
10.1029/2024JD041447

Observed Responses of Gravity Wave Momentum Fluxes to the Madden–Julian Oscillation Around the Extratropical Mesopause Using Mohe Meteor Radar Observations

Xu Zhou[1], Libo Liu[1,2,3], Xinan Yue[1,2,4], Guiwan Chen[5], and Xian Lu[6]

[1]Key Laboratory of Earth and Planetary Physics, Institute of Geology and Geophysics, Chinese Academy of Sciences, Beijing, China, [2]College of Earth and Planetary Sciences, University of Chinese Academy of Sciences, Beijing, China, [3]Heilongjiang Mohe National Geophysical Observatory, Institute of Geology and Geophysics, Chinese Academy of Sciences, Beijing, China, [4]Beijing National Observatory of Space Environment, Institute of Geology and Geophysics, Chinese Academy of Sciences, Beijing, China, [5]State Key Laboratory of Numerical Modeling for Atmospheric Sciences and Geophysical Fluid Dynamics, Institute of Atmospheric Physics, Chinese Academy of Sciences, Beijing, China, [6]Department of Physics and Astronomy, Clemson University, Clemson, SC, USA

Key Points:

- The 12-year observations of the Mohe meteor radar revealed prominent intraseasonal variations in gravity wave momentum fluxes (GWMFs)
- The GWMF increased by ∼2–4 m^2/s^2 during Madden–Julian oscillation (MJO) Phase 4 (P4), leading to the response of zonal winds to approximately 2 MJO phases (1/2π)
- Time-lagged composites revealed enhanced westward GWMFs lagging MJO P4 ∼25–35 days, suggesting a possible mechanism via planetary waves

Correspondence to:
X. Yue,
yuexinan@mail.iggcas.ac.cn

Citation:
Zhou, X., Liu, L., Yue, X., Chen, G., & Lu, X. (2024). Observed responses of gravity wave momentum fluxes to the Madden–Julian oscillation around the extratropical mesopause using Mohe meteor radar observations. *Journal of Geophysical Research: Atmospheres*, *129*, e2024JD041447. https://doi.org/10.1029/2024JD041447

Received 26 APR 2024
Accepted 26 OCT 2024

Author Contributions:
Conceptualization: Xu Zhou, Guiwan Chen
Data curation: Libo Liu
Formal analysis: Xu Zhou
Funding acquisition: Xu Zhou, Xinan Yue
Investigation: Xu Zhou
Methodology: Xu Zhou
Supervision: Xinan Yue
Validation: Xu Zhou
Visualization: Xu Zhou
Writing – original draft: Xu Zhou
Writing – review & editing: Xu Zhou, Libo Liu, Xinan Yue, Guiwan Chen, Xian Lu

Abstract The 12-year continuous observation of gravity wave momentum fluxes (GWMFs) estimated by the Mohe meteor radar (53.5°N, 122.3°E) revealed prominent intraseasonal variability around the extratropical mesopause (82–94 km) during boreal winters. Composite analysis of the December–January–February (DJF) season according to the Madden–Julian Oscillation (MJO) phases revealed that the zonal GWMFs notably increased in MJO Phase 4 (P4) by ∼2–4 m^2/s^2, and a Monte Carlo test was designed to examine the statistical significance. The response in zonal winds lags behind the GWMF response by two MJO phases (i.e., 1/2π), indicating a "force–response" interaction between them. Additionally, time-lagged composites revealed that strengthened westward GWMFs occurred ∼25–35 days after MJO P4, coincident with the MJO impact on the zonal winds in the stratosphere. The analysis results also suggested that the mechanism of MJO by which the MJO influences the stratospheric circulation might involve poleward propagating effects of stationary planetary waves with zonal wavenumber one. This work emphasizes the importance of GW intraseasonal variability, which impacts tropical sources from the troposphere to the extratropical mesopause.

Plain Language Summary Atmospheric gravity waves (GWs) are small-scale high-frequency perturbations that are important for the circulation in the middle atmosphere. GWs originate from the troposphere and propagate upward into the mesosphere, eventually breaking down and transporting momentum fluxes (GWMFs) to background winds. One of the tropospheric sources is convection, which has a dominant intraseasonal variation mode in the tropical region, named Madden–Jullian Oscillation (MJO). This work investigates how tropical GW sources impact the extratropics, using 12-year continuous observations by the Mohe meteor radar (53.5°N, 122.3°E). Obvious intraseasonal signals in the GWMF are found during northern winter. The GWMF data were then composited with respect to the MJO phases. Notable increases were observed when the MJO convection is enhanced over the Indian Ocean. The zonal wind response is obviously positive when the MJO is active over the Western Pacific Ocean, which occurs after the GWMF response. This result indicates an interaction between the GWMF and background winds by the MJO modulation. Furthermore, we examined GWMF responses to the MJO at different lag times, and the lagged response coincided with the background wind response in the stratosphere. The stratospheric wind variation is found to be modulated by poleward-propagating planetary waves.

1. Introduction

Gravity waves (GWs) are essential processes in the dynamics of the entire atmosphere, carrying momentum and energy from the troposphere upward to the middle and upper atmosphere (Vadas et al., 2014). As GWs reach the mesopause, they may break down and dissipate, eventually depositing momentum fluxes into the mean flow (Fritts & Alexander, 2003). Thus, the variability in GW momentum fluxes (GWMFs) around the mesopause is an important issue for the research community. Previous investigations have advanced our understanding of GWMF variabilities at time scales ranging from days to years, which are mostly explained physically by changes in wave sources and background winds in the propagating pathway (de Wit et al., 2016; Liu et al., 2013; Placke et al., 2011). The tropospheric origins include orography, wind shear, convection, etc. Generally, convection is

the main GW source in the tropics, whereas orographic sources are essential in the extratropics. Recently, increasing evidence has revealed that variations in tropical wave sources can influence weather systems outside the tropics and establish tropical–extratropical teleconnections via the modulation of wave propagation or other nonlinear processes (Domeisen et al., 2019; Kang & Tziperman, 2018; Lin et al., 2009; Salminen et al., 2020; Zhou et al., 2020). The question of whether and how tropical heating sources influence GW variability over the extratropics therefore is of increasing interest to researchers.

The Madden–Julian Oscillation (MJO; Madden & Julian, 1971, 1972) is one of the dominant intraseasonal variabilities in the tropical troposphere and is represented by the eastward-propagating pattern of coupled convection–circulation systems around the equatorial region (Zhang, 2005). Although the slow-moving MJO is confined to the low-latitude lower atmosphere mainly due to the moisture availability in the tropics and the small value of the Coriolis parameter, the influences of the MJO can extend to the extratropics (Cassou, 2008; Sun et al., 2021; Vitart & Molteni, 2010) and upward to the middle and upper atmosphere (Gasperini et al., 2020; Kumari et al., 2020, 2021; Liu et al., 2018; Zhou et al., 2023) via poleward- and upward-propagating waves. Early works reported MJO-like signals in the equatorial mesosphere and lower thermosphere (MLT) winds, which are suggested to be modulated by GWs and atmospheric tides (Eckermann et al., 1997; Eckermann & Vincent, 1994). Modern satellite observations have also revealed the MJO–GW relationship in the tropical stratosphere (Alexander et al., 2018; Moss et al., 2016; Tsuchiya et al., 2016). For the global responses in the middle atmosphere, Li and Lu (2020) recently discussed MJO modulation on GW variances based on the SABER temperature observations. The authors also suggested that different mechanisms dominated in the tropics and extratropics. Furthermore, an analysis of parameterized GW drag based on reanalysis data has revealed that GW drag drives zonal wind as a forcing term and thus produces a $1/2\pi$ phase difference (two MJO phases with respect to the total eight MJO phases) ahead of zonal-wind responses, which is simplified as a "force–response" system (Li & Lu, 2021). The MJO modulation on wave sources is crucial for GW generation, and the teleconnection between the MJO and the stratosphere is suggested to play an essential role in GW propagation. Alexander et al. (2018) proposed that stratospheric waves and tropopause wind anomalies follow MJO-related precipitation sources. GWs with long vertical wavelengths are also sensitive to variations in stratospheric zonal winds, but are only weakly impacted by tropopause wind variations.

Previous investigations have discussed how MJO activities affect the stratosphere, particularly by disturbing the stratospheric polar vortex in the Northern Hemisphere (NH). MJO-related tropical heating generates subtropical planetary waves (PWs) that propagate poleward and are known to affect tropospheric weather systems in the NH (e.g., Cassou, 2008). Garfinkel et al. (2012, 2014) reported that these poleward waves can also propagate upward into the stratosphere and induce temperature anomalies. Approximately 10 days after MJO-related convection is enhanced over the central Pacific Ocean (Phase 7), warm temperature anomalies form in the NH polar lower stratosphere. On the basis of National Center for Environmental Prediction-National Center for Atmospheric Research (NCEP-NCAR) reanalysis data, Liu et al. (2014) also revealed a similar relationship between the polar vortex and the MJO; this Arctic circulation pattern tends to have a zonal structure of wavenumber-1 or wavenumber-2 ~25–30 days after the MJO is active over the Indian Ocean (Phase 3). Wang et al. (2018) reported that the high occurrence of convection anomalies over the Maritime Continent (MJO P4) depressed wave activity and led to a stronger polar vortex in the middle and upper stratosphere. The authors suggested that the influence of the MJO is related to the excited poleward Rossby waves in MJO P4, which are antiphase with wavenumber-1 stationary PWs at mid-to high-latitudes. Using idealized model experiments, Kang and Tziperman (2017) identified two teleconnection mechanisms explaining the MJO influence on the polar vortex: (a) direct propagation of MJO-forced transient waves to the Arctic stratosphere and (b) nonlinear intensification of stationary waves by MJO-forced transient waves. They also noted that the time scale of poleward wave propagation is approximately 10–20 days, whereas the additional time for the subsequent upward wave propagation is still uncertain. However, the GWs in the MLT region, which is sensitive to stratospheric zonal winds, in response to the MJO are still poorly understood.

The Mohe meteor radar (53.5°N, 122.3°E) has been continuously monitoring MLT dynamics for 12 years. These continuous observations provide an opportunity to analyze the intraseasonal variability of the extratropical GWMF and to examine the potential MJO-related impacts around the mesopause. In this study, we apply the approach of Hocking (2005) to derive the GWMFs at 82–94 km and then examine the intraseasonal variability, explore the MJO modulation, and propose a possible interpretation.

2. Data and Methodology

2.1. Mohe Meteor Radar Observations

The Mohe meteor radar is located in extratropical East Asia (53.5°N, 122.3°E), latitudinally between the tropics and the Arctic polar vortex. The radar has accumulated observational data since August 2011 and is routinely operated and maintained by the Institute of Geology and Geophysics, Chinese Academy of Sciences. The radar is a conventional atmospheric radar system (manufactured by ATRAD) that transmits a radio wave frequency of 38.9 MHz with a peak power of 20 kW. The peak height of the detected meteor events is ∼90 km.

Owing to the Doppler shift from the echoes of meteor trails, which are carried by neutral winds, meteor radars allow us to measure the radial velocities and determine the vector winds. Hocking (2005) proposed a least-square fitting approach to estimate the GWMF using the radial velocities measured by meteor radar for the first time, and this approach has since been widely used for research (Andrioli et al., 2013; Fritts et al., 2010; Jia et al., 2018; Liu et al., 2013; Pramitha et al., 2020; Vincent et al., 2010). Zhou et al. (2022) applied the processing method to the Mohe meteor radar and evaluated the performance with necessary error and uncertainty analysis. The good data quality and adequate data volume indicate that the Mohe meteor radar observations can provide a reasonable estimate of the GWMF at heights ranging from 82 to 94 km each month. In this study, we shorten the composite window from one month to 11 days with a 1-day step, which still ensures sufficient data points for the least-squared fitting as proposed by Vincent et al. (2010). The data in each composite window are binned into 2-hr local-time and 3-km height grids with steps of 1-hr and 1-km to derive the mean winds and GWMFs. The daily mean value of the GWMF was then used for further analysis. Notably, we reduced the spurious contributions of tides and 2-day waves in the GWMF estimation, which is the same process used by Zhou et al. (2022). PWs with longer periods were not considered, given that those long-period waves do not change significantly in the 2-hr local-time bin and thus introduce limited spurious variance.

2.2. Analysis Methodology

We followed the methods of Yang et al. (2018) and Kumari et al. (2021) to examine the GWMF responses to the MJO. The daily GWMF was filtered by a bandpass window of 30–90 days for focus on subseasonal timescales. Then, active MJO events were determined according to the criterion of the Real-time Multivariate (RMM) MJO index (https://psl.noaa.gov/mjo/mjoindex/; Wheeler & Hendon, 2004), which has an amplitude larger than 1.0 for at least five consecutive days. The threshold of 1.0 is commonly used in distinguishing the active MJO events (e.g., Barrett et al., 2021). We did not choose a stricter threshold value, such as 1.5 in Yang et al. (2018), because our data coverage was not as long as that used in their study. The MJO amplitudes and phases were diagnosed by the first two components of the RMM MJO index, RMM1 and RMM2. The MJO amplitude was calculated by the square root of the sum of RMM1 and RMM2, and eight different MJO phases (labeled from 1 to 8) are defined according to the tangent values of the ratio of RMM1 to RMM2. The different MJO phases also indicate the longitude sectors where the MJO is enhanced. The filtered GWMFs during the active MJO events were assigned to each MJO phase and then binned to yield the composite anomalies. This work focuses on the boreal winter season (December–January–February, DJF) during which the MJO is most active. In addition, the data from the first and last 3 months was removed from the bandpass-filtered time series in the composite analysis, and the interannual variability was not considered.

In addition, a Monte Carlo test based on bootstrap sampling with replacement was designed to examine the statistical significance of the results. The daily GWMF was randomly sampled 500 times to form a new time series, and then composite analysis was performed on each series. The standard deviation of the derived 500 composite values thus represents the "noise" level for each MJO phase. If the composite value from the "true" observation is greater than twice the "noise" level, it is regarded as statistically significant (95%).

2.3. ECMWF-ERA5

In this paper, the ECMWF Reanalysis v5 (ERA5; Hersbach et al., 2020) data set is used to examine wind variation below and to discuss the possible mechanism by which the GWMF responds to the MJO. ERA5 is produced on the basis of the 4D-Var data assimilation system, which combines various historical observations into the ECMWF Integrated Forecast System (IFS). The high-top CY41R2 ECMWF IFS model includes 137 hybrid pressure levels vertically ranging from the surface (1,000 hPa) to ∼80 km (1 Pa). A postprocessed product of the

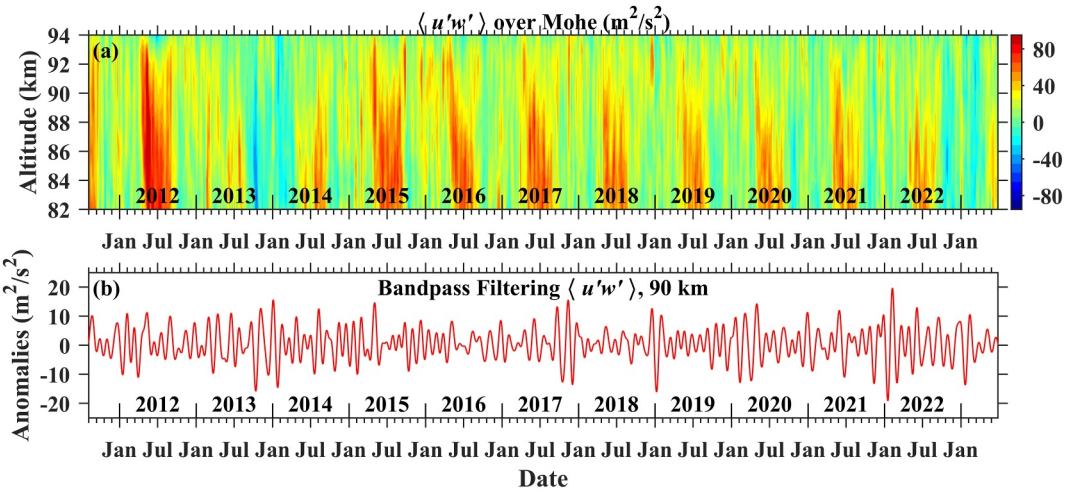

Figure 1. (a) Temporal evolution of zonal GW momentum fluxes $\langle u'w' \rangle$ over the Mohe radar at 82–94 km. (b) The 30–90days bandpass filtering $\langle u'w' \rangle$ at 90 km.

ERA5 data set for quick access is available on the cloud server (https://cds.climate.copernicus.eu/), and this product provides global atmospheric parameters (e.g., temperature, pressure, and wind) at 37 pressure levels from 1,000 hPa to 1 hPa (~50 km). In general, the state-of-the-art ERA5 data set describes low-frequency climate variability from 10 hPa downward well and matches other reanalysis data sets (e.g., MERRA-2 and JRA-55). Previous studies have also comprehensively evaluated the characterization of the ERA5 data set on MJO precipitation, circulation, and the energy budget (Hsiao et al., 2020; Ren et al., 2021). For detailed information, refer to Hersbach et al. (2020) and https://www.ecmwf.int/en/forecasts/dataset/ecmwf-reanalysis-v5.

3. Results

3.1. Intraseasonal Variability

Figure 1a shows the temporal variation in the zonal GWMF, $\langle u'w' \rangle$, estimated by the Mohe meteor radar at 82–94 km. Strong eastward GWMFs could be found in boreal summer, which results from the westward prevailing winds. The prominent intraseasonal variability is superimposed on the seasonal variation. Figure 1b displays the 30–90 days bandpass-filtered result of $\langle u'w' \rangle$ at 90 km. The amplitude reaches ~20 m^2/s^2 and generally has large values in boreal winter. The Morlet-wavelet spectrum (Figure 2a) illustrates the frequency characteristics of the nonfiltered GWMF variability (Yamazaki, 2023). The wavelet spectrum is based on the daily GWMF estimated every 11 days, so variability with a shorter period is not recognized. The black contours in the wavelet spectrum indicate that the limit value has reached 95% significance. The intraseasonal variability shows a clear seasonal dependence, being less pronounced in boreal summer compared to boreal winter. Prominent intraseasonal variability with periods of ~50–60 days can be found in the boreal winters of 2013/2014, 2017/2018, 2019/2020, and 2021/2022. To focus on the frequency characteristics during the DJF seasons, Figure 2b displays the Lomb-Scargle periodogram for each boreal winter and the averaged spectra, and a significant peak is found at approximately 33 days. Having demonstrated the strong intraseasonal variability of GWMFs, especially for the boreal winter season, we further analyze the responses to MJO activity and focus on the DJF season.

3.2. MJO Phase Modulation

Figure 3a illustrates the composite anomalies of the zonal GWMF according to the MJO phases during the DJF season. The shaded area indicates a 95% significance compared with the "noise" level examined by the Monte Carlo test described in Section 2.2. Significant positive responses are found in MJO Phase 4 (P4), which reaches values of ~2–4 m^2/s^2. Compared with the DJF mean value of 15–20 m^2/s^2, the positive anomalies are ~15%–25%. The composite anomalies are slightly negative in MJO P8–P1 (~−1–−3 m^2/s^2). Positive responses occur in P2 and P7, but the strength is not strong enough with respect to the noise level, that is, they are insignificant. The composite anomalies of the zonal winds are also examined, considering that the GWMF is the main force driving

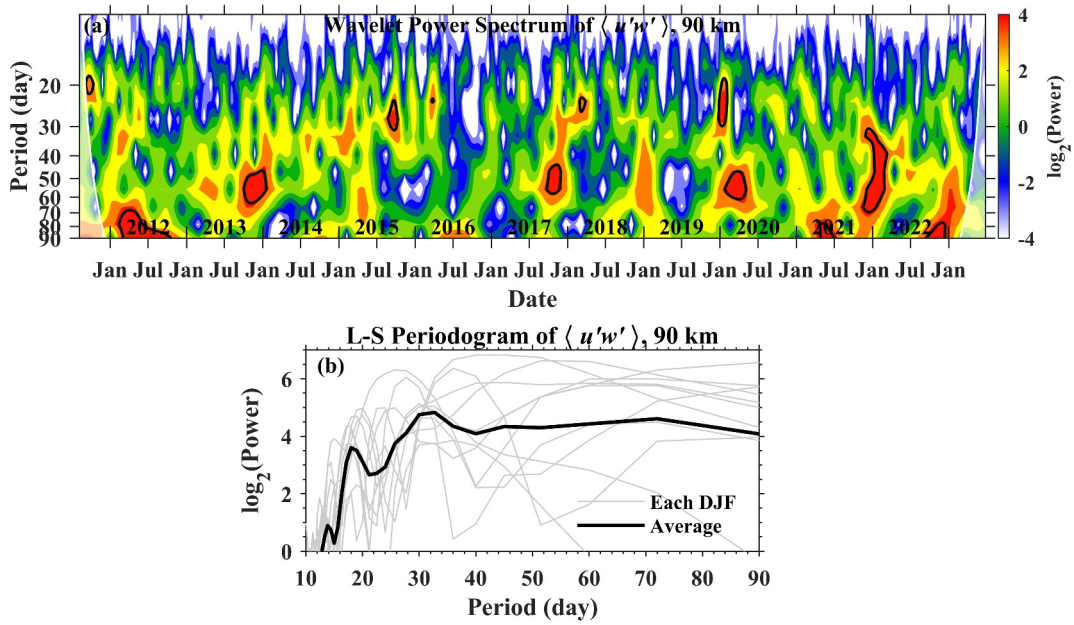

Figure 2. (a) Wavelet power spectrum of $\langle u'w' \rangle$ at 90 km. The gray shading indicates the cone of influence for the wavelet analysis, and the black contours represent a 95% confidence level. (b) The Lomb-Scargle periodogram of zonal GW momentum fluxes during each DJF season is shown as gray lines, and the averaged spectrum is shown with the black line.

the changes in zonal winds around the mesopause. The responses of zonal winds to MJO phases are more distinct than those of the zonal GWMF, partly because the error and uncertainty in the wind observations are much smaller. The much clearer "wave-1" structure versus the MJO phases is shown in Figure 3b; the zonal winds tend to be larger in P6 (+3 m/s) and smaller in P2 (−3 m/s). The maximum responses in the zonal winds occur two MJO phases later than those in the GWMF.

To interpret the different MJO-phase responses in the zonal winds and zonal GWMFs, we present Equation 1 and describe how $\langle u'w' \rangle$ affects the tendency of zonal winds,

$$\frac{\partial U}{\partial t} = -\frac{1}{\rho}\frac{\partial \rho \langle u'w' \rangle}{\partial z} = \left[\frac{1}{H} - \frac{\partial}{\partial z}\right]\langle u'w' \rangle \tag{1}$$

where ρ is the mass density, and H is the scale height. $\langle u'w' \rangle$ acts as a forcing term, and U is the corresponding response term. Both the forcing and response terms have a "wave-1" structure with respect to the MJO phases, as shown in Figures 3a and 3b, and the wave-1 fitted function can be expressed as,

$$U \equiv A_u e^{i(\omega t - \varphi_u)} \tag{2.1}$$

$$\langle u'w' \rangle \equiv A_{GW} e^{i(\omega t - \varphi_{GW})} \tag{2.2}$$

where A_u and A_{GW} are the amplitudes, and where φ_u and φ_{GW} are the phases of the zonal winds and zonal GWMFs, respectively. ω is the angular frequency, corresponding to $\frac{2\pi}{8\ \mathrm{MJO-phases}}$. With substitution of the fitted function into Equation 1, the relationship between the anomalies of zonal GWMFs and zonal winds can be described as follows:

$$\omega A_u e^{i(\omega t - \varphi_u + \pi/2)} = \left[\frac{1}{H} - \frac{\partial}{\partial z}\right] A_{GW} e^{i(\omega t - \varphi_{GW})} \tag{3}$$

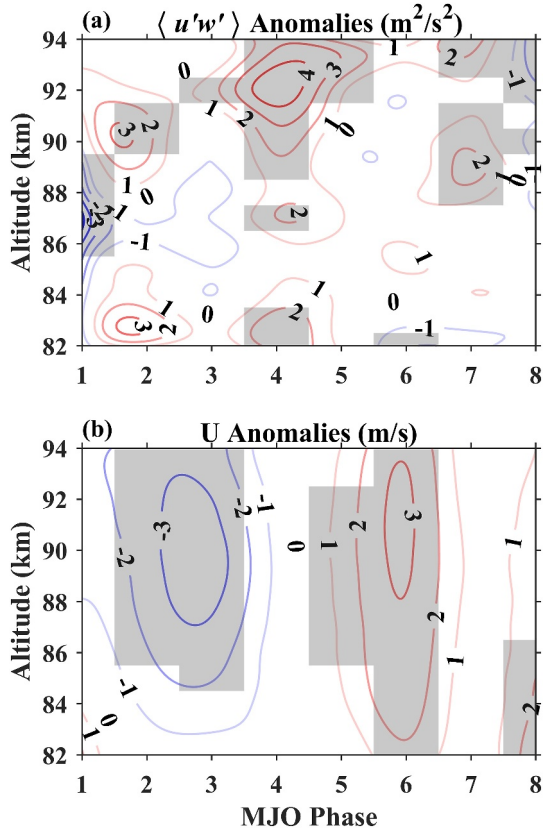

Figure 3. Anomalies of (a) $\langle u'w' \rangle$ and (b) zonal winds during the December-January-February (DJF) season estimated from Mohe meteor radar observations. The shaded areas indicate the results at the 95% significance level.

If the GWMF amplitude does not have a wave-like structure vertically, that is, if the term $\partial / \partial z$ does not produce an imaginary part, the phases of the zonal winds and zonal GWMF should exhibit the following relationship,

$$\varphi_{GW} = \varphi_u - \frac{\pi}{2} \tag{4}$$

In other words, the zonal GWMF should lead the zonal winds in the MJO responses with a phase of π/2. Figure 4 examines the relationships by illustrating the wave-1 fits. According to the fitting analysis, φ_u lags φ_{GW} by approximately 0.487π. This result agrees well with the aforementioned theoretical prediction, indicating that the dominant interaction between zonal winds and zonal GWMFs responding to the MJO is captured. The slight discrepancy might come in part from the assumption of no vertical wave-like structure in the theoretical derivation or observational uncertainties. The π/2 phase lag in the response term to the forcing term is similar to the interaction between GWs and the quasi-biennial oscillation (QBO; Baldwin et al., 2001) and the relationship between GWs and diurnal tides (Liu et al., 2013), whereas this study revealed such a "force–response" system on the intra-seasonal timescale.

3.3. Mechanism Interpretation

To explore the mechanism of GW responses to the MJO shown in Figures 3 and 4, we further examine the responses of zonal winds in the stratosphere to changes in MJO phases, considering that GW variability is closely modulated by changes in stratospheric background winds due to the well-known "critical-level filtering" (Fritts & Alexander, 2003). The critical-level filtering theory suggests that background winds absorb GWs with the same phase speed and thus prevent those GWs from propagating further. Figure 5 shows the climatological profiles of seasonal mean zonal winds over Mohe, as provided by the ECWMF ERA-5 data set. The DJF zonal winds are eastward for all altitudes from 0 to 80 km, indicating that GWs with westward momentum fluxes are more likely to propagate into the mesosphere. Based on the ERA-5 reanalysis data set, the anomalies of zonal-mean zonal winds at pressure levels of 1–100 hPa (altitudes of approximately 15–50 km) in response to different MJO phases are illustrated in Figure 6a. In the upper stratosphere (pressure level <10 hPa, altitudes >∼30 km) over Mohe,

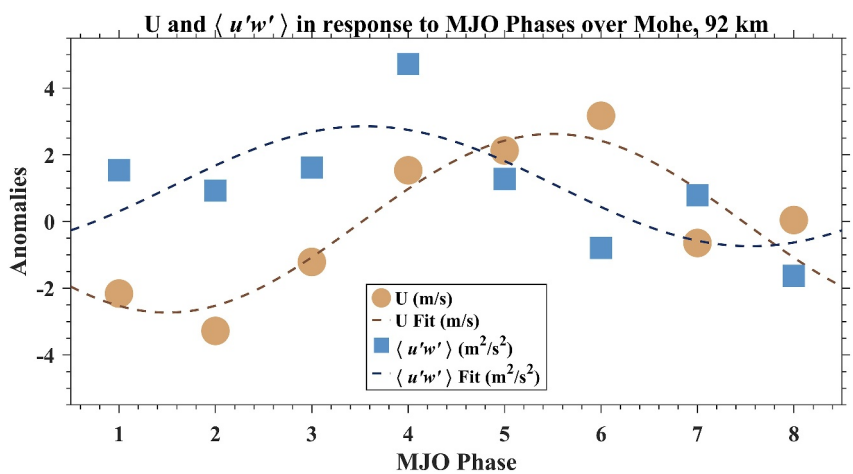

Figure 4. Anomalies of zonal winds (brown dots) and zonal GWMF (blue squares) in response to MJO phases at 92 km. The brown and dark blue dashed lines indicate the wave-1 fit.

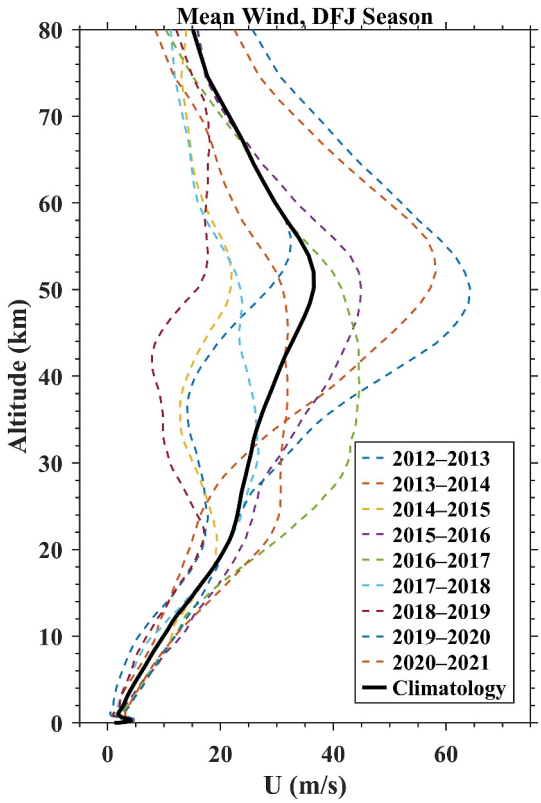

Figure 5. The DJF-season averaged zonal winds over Mohe provided by the ERA5 reanalysis data.

positive anomalies are found in MJO P1–P4, and negative anomalies are found in MJP P5–P8. The stratospheric wind responses to the MJO phases agree with the results of Li and Lu (2021) based on MERRA-2 reanalysis data. The enhanced eastward stratospheric zonal winds in MJO P1–P4 lead to westward GWs propagating upward, whereas the GWMF anomalies around the mesopause shown in Figure 3a do not correspond to this in-phase. Li and Lu (2021) presented similar results and stressed that the interaction between GW drag and wind plays a role in the out-of-phase relation. Both positive and negative anomalies in zonal winds occur 1–2 MJO phases later in the lower stratosphere (pressure levels of 10–100 hPa) than in the upper stratosphere. The downward propagation of stratospheric wind responses proceeds with the MJO phases, which also suggests the similarity between the MJO-GW interaction and the QBO-GW interaction to some extent (Baldwin et al., 2001). Some previous investigations have also suggested that, aside from the zonal winds in the stratosphere, zonal winds in the lower mesosphere could also affect gravity waves and the mean flow above (Becker & Fritts, 2006). This viewpoint was also used by Karlsson et al. (2008, 2009) to explain the variability of polar mesospheric clouds (PMCs) in the summer polar mesopause, and by Li et al. (2016) to interpret how the El Niño–Southern Oscillation (ENSO) affects the mesosphere polar region. In Li & Lu (2021), the responses of zonal winds in the mesosphere to the MJO phases were shown to lead the stratospheric responses. The positive responses of zonal winds in the stratosphere gradually become slightly negative at around 80 km. This might also contribute to the positive GWMF anomalies in the responses shown in Figure 3a. Our result is also consistent with previous work by Wang et al. (2018) using NCEP–NCAR reanalysis data, which demonstrated that the enhanced polar vortex is associated with the higher-frequency occurrence of MJO P4. Figure 6b illustrates the composite anomalies at the pressure level of 10 hPa, which are positive during MJO P7–P3 at 30°N and exhibit poleward progression in MJO P1–P4 at 60°N. The different anomalies associated with different MJO phases in the vertical-latitudinal plane suggests that there should be a lag response between the zonal-mean zonal winds over the extratropics and the MJO source in the tropics.

Figure 7a shows the effects on the zonal-mean zonal winds for different lags after MJO P4. The composite anomalies in the extratropics are significantly negative for lags of 25–40 days (~4 m/s). The maximum negative anomalies at 50°N lead ~5 days to those at 60°N, so the lags of tropical MJO sources arriving in the northern extratropics, including the Mohe radar site, should be ~25 days according to simple linear estimation. The time-lagged composite analysis on the zonal-mean zonal winds also confirmed the argument proposed by Li and Lu (2020) that the NH polar vortex should weaken 25–40 lag days following MJO P4. The strength of the polar

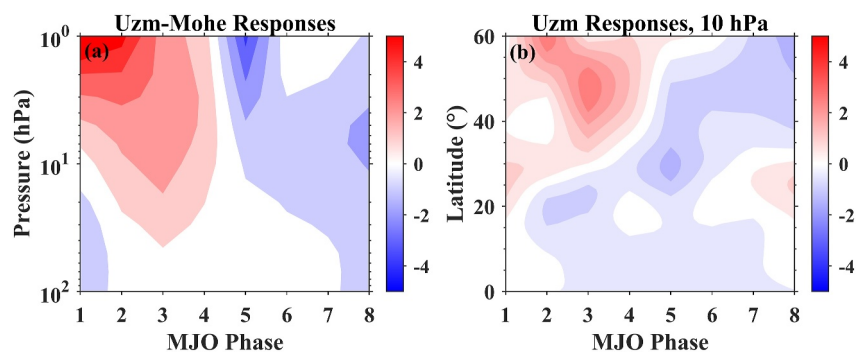

Figure 6. (a) Responses of zonal-mean zonal winds over the latitude of the Mohe radar site to the changes in the MJO phase during the DJF season at different pressure levels estimated from the ERA-5 reanalysis data set. (b) Responses of zonal-mean zonal winds at 10 hPa for different latitudes.

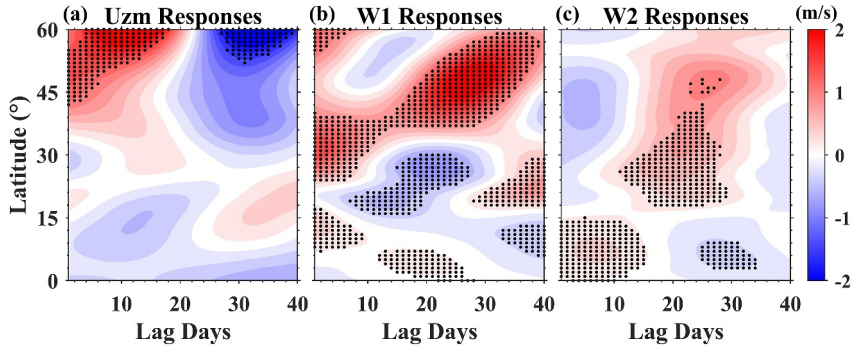

Figure 7. (a) Anomalies of zonal-mean zonal winds at the pressure level of 10 hPa for different lag days after MJO P4 during the DJF season. The black-dotted areas indicate the results with a 95% significance level. Plots (b) and (c) are the same as plot (a) but for the amplitudes of wavenumber-1 and wavenumber-2 stationary PWs in zonal winds, respectively.

vortex can be determined from various proxies, and one of most commonly used proxies is the zonal-mean zonal winds (Charlton & Polvani, 2007). Stronger eastward winds at 60°N and 10 hPa indicate a more stable polar vortex. The anomalies of stationary wavenumber-1 and wavenumber-2 PW amplitudes in zonal winds for different lags after MJO P4 are illustrated in Figures 7b and 7c, respectively. Larger anomalies in the wavenumber-1 PW amplitude appear at midlatitudes (~35°N–40°N) approximately 15 days after MJO P4 and extend to highlatitudes (~60°N) as the lag days increase. The anomalies in the wavenumber-2 PW amplitude are relatively weak and are constrained mainly to the mid-to-low latitudes; therefore, they are insignificant at the latitudes of Mohe (53.5°N). The analysis indicates that the poleward planetary waves should play a role in modulating the anomalies of zonal-mean zonal winds, especially for the wavenumber-1 component. The importance of wavenumber-1 PW was also examined by Sun et al. (2021), who provided a comprehensive analysis of the E–P flux and the E–P flux divergence of PWs. The E–P flux is commonly used to diagnose the propagation of PWs and the forcing on the zonal-mean flow. Sun et al. (2021) reported that, about 30–35 days after convection anomalies over the Maritime Continent (P4), enhanced PWs decrease the E–P flux divergence and thus lead to weaker eastward zonal winds in the upper stratosphere and lower mesosphere. Kang and Tziperman (2017) also reported that an enhanced stationary PW with wavenumber-1 can reach the stratosphere and modulate winds.

The responses of the zonal-mean zonal winds in the stratosphere to the MJO analyzed above suggest that the polar vortex tends to be weak, lagging the MJO P4 by approximately 25–35 days. The weakened polar vortex leads to less critical level filtering of GWs, and stronger GW activities are thus expected to occur above and give rise to a more westward GWMF. In Figure 8, the time-lagged composite anomalies of the zonal GWMF around the mesopause for individual MJO phases are shown. Significant negative anomalies are observed ~25–35 days after MJO P4 ($-3\ m^2/s^2$), that is, more westward GWMFs arose. This result is in line with the expectations mentioned above, and it is suggested that the mechanism by which the MJO influences the extratropical GWMF around the mesopause involves modulation by the stratospheric circulation below.

4. Discussion

This work explores the intraseasonal variability of the zonal GWMF around the mesopause over an extratropical location near the edge of the northern polar vortex, the Mohe radar site (53.5°N, 122.3°E), in response to the MJO sources in the tropical troposphere. Analysis via bandpass filtering revealed that significant intraseasonal variability in zonal GWMFs occurred during boreal winters. The composite anomalies of the zonal GWMF response to individual MJO phases are significantly positive in MJO P4, leading the zonal-wind responses by two MJO phases (1/2π phase ahead). Equations 1–4 interpret the different MJO-phase responses in the zonal GWMF and zonal winds, indicating that their interaction acts as a "force–response" system. We further propose a possible mechanism for interpreting how the tropical MJO source influences extratropical GWs. Analysis of the ERA-5 data revealed that the zonal-mean zonal winds in the stratosphere are modulated by the individual MJO phases. The stratospheric circulation becomes weak after a lag of 25–35 days following MJO P4, which might be influenced by the tropical MJO via the poleward wavenumber-1 PW. The weakened stratospheric circulation

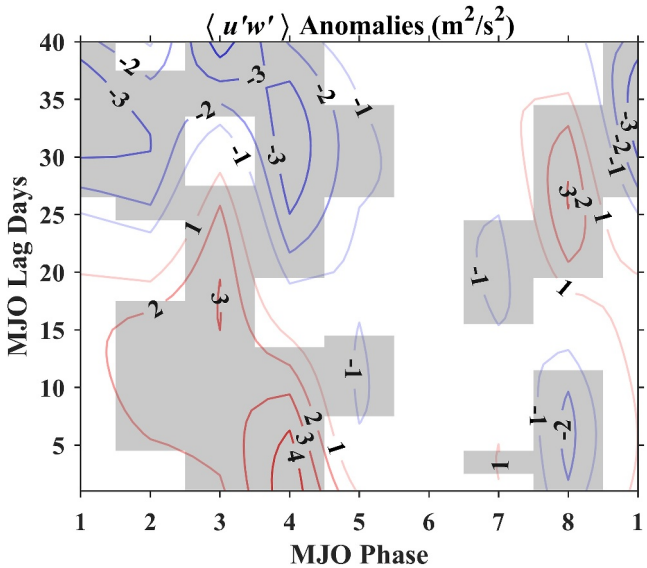

Figure 8. Anomalies of $\langle u'w' \rangle$ at 92 km for different lags after the various MJO phases 1–8 during the DJF season. The shaded areas indicate the results with a 95% significance level.

leads to less critical layer filtering of GWs and thus modulates the strength of the zonal GWMF around the mesosphere.

The significant intraseasonal variability in the zonal GWMF does not coincide one-to-one with the strong intraseasonal signal in zonal winds. As demonstrated by Gong et al. (2022), the 2015/2016 winter exhibited a prominent intraseasonal oscillation (ISO) in zonal winds, but no such strong ISO in the GWMF was detected during the same period. The results suggest that the relationship between winds and the GWMF is not a case-to-case response, as other sources can contribute to them separately. For instance, the strong ISO in the GWMF during January 2022 might be related to the eruption of Tonga volcano (Liu et al., 2022). This is also the reason why composite analysis according to the MJO phase is necessary. The method could suppress other contamination effects and highlight the MJO-related "spectrum." For another example, the 27-day solar cycle might modulate GW variability (Cullens et al., 2016), but it should produce limited effects in our analysis of the responses to the MJO due to the data processing.

Similar 1/2π phase differences in the zonal GWMF and zonal wind responses to the MJO were also noted by Li and Lu (2021). They investigated the relationship between wind and parameterized GW drag. The GWMFs produce the GW drag acting on the zonal winds, as shown in Equation 1, but these two quantities are not identical. The present work provides direct evidence from observations rather than from parameterization. A similar "force–response" system between the background winds and GW forcing can also be found in the other atmospheric variabilities, for example, the semiannual oscillation (Ern et al., 2021) and QBO (Ern et al., 2014) in the equatorial middle atmosphere.

With respect to the mechanism by which the tropical MJO source affects stratospheric winds in the NH extratropical region, some investigations focused on this phenomenon and have suggested the modulation of poleward propagating transient waves and stationary PWs. Garfinkel et al. (2012, 2014) reported that the wavenumber-1 heat flux after enhanced convection anomalies over the central Pacific Ocean (MJO P7) is in phase with climatological stationary waves, and thus weakens the polar vortex. The temperature anomalies occurred in the stratosphere ∼30 days after MJO P4, which is consistent with the results in this paper. Wang et al. (2018) suggested that convection anomalies over the Maritime Continent (MJO P4) can excite a Rossby wave train that propagates poleward, which is antiphased with climatological stationary waves, decreases wave activity and leads to a stronger polar vortex in the middle and upper stratosphere. Kang and Tziperman (2017) suggested that both MJO-forced transient waves and stationary waves are important in teleconnections. In addition to the MJO-induced transient wave propagating upward and poleward, the stationary PW with wavenumber-1 can also be enhanced and reach the stratosphere. The enhanced stationary wave heat flux in the NH stratosphere changes the stratospheric winds and the SSW frequency. Sun et al. (2021) emphasized the importance of enhanced stationary PWs after MJO P4, which can propagate upward into the upper stratosphere and mesosphere, induce temperature anomalies and lead to weaker eastward zonal winds. In our analysis, the composite anomalies of stratospheric zonal winds (Figure 6) confirmed that the strong polar vortex appears in MJO P2–P4, and the time-lagged analysis further illustrated that a weakened polar vortex occurs ∼25–35 days after MJO P4. We also found that a weakened stratospheric wind after MJO P4 should be associated with the enhanced wavenumber-1 stationary PW (Figure 7).

As a weakened polar vortex occurred after MJO P4, our results further revealed significant negative anomalies in the GWMF approximately 25–35 days after MJO P4 (Figure 8). Other investigations have confirmed a similar relationship between the polar vortex and mesospheric GW activities above (e.g., Li et al., 2020; Li & Lu, 2020; Triplett et al., 2018). Triplett et al. (2018) suggested that compared to a stable vortex, a weaker or more variable polar vortex tends to cause GWs to break up over greater depths and lower altitudes (Becker, 2004). Our analysis indicates that the mesopause GWMF response to the MJO phase is likely related to MJO modulation on the stratospheric polar vortex, which influences the GWMF above. However, in this work, we ignored the GW forcing on polar vortex deceleration (e.g., Gupta et al., 2021; Song et al., 2020).

Considering the connection between the MJO and SSW in winter (e.g., Garfinkel et al., 2012, 2014) and the SSW impacts on GWs (e.g., Thurairajah et al., 2014), we also examine whether the occurrence of SSW has potential impacts on our analysis results. Yang et al. (2019) reported that the NH stratospheric responses after MJO P2 and P3 would be much weaker if the data during the ±50 days before and after major SSW events were excluded. In this study, three major SSW events occurred in the DJF seasons during the period we investigated, that is, Jan 2013 Feb 2018, and Jan 2021. We reanalyzed the zonal GWMF responses to the MJO, excluding the winters with SSW events. When the data of the remaining eight DJF winters are used, the positive response in MJO P4 is still statistically significant (not shown) and the main features are not obviously different from those in Figure 3. The responses in MJO P2 and P3 also do not become significantly weak as sensitively as suggested by Yang et al. (2019). However, if the data could cover many more SSW events, we could examine the potential SSW effects more comprehensively.

However, several aspects need to be improved upon in the future. For example, we did not distinguish slow and fast MJO cases because of the existing data coverage, whereas Yadav et al. (2024) revealed that they have different effects on the stratosphere. In their work, almost 40-year data were used, so there were adequate sample sizes for both slow and fast MJO episodes for analysis. In addition, this work provided a statistical insight into the GW variability around the extratropical mesopause modulated by MJO phases, but the sensitivity to the MJO strength was still unknown. Model simulation should be a powerful tool for further investigation; however a realistic situation that needs to be considered is that the simulated connection between the MJO and vortex variability in most mainstream models is weaker than the observed connection (Schwartz & Garfinkel, 2020).

5. Conclusion

On the basis of the 12-year continuous observations by the Mohe meteor radar (53.5°N, 122.3°E), we estimated the GWMFs and investigated the prominent intraseasonal variability during boreal winters. The results provide direct observational evidence that connects the GWMF around the extratropical mesopause and tropical MJO activity in the troposphere. The composite analysis during the DJF season revealed notable positive GWMF responses to MJO P4, with a maximum magnitude of 2–4 m^2/s^2 at ∼92 km, with a greater than 95% significance level determined via a Monte Carlo test. The zonal wind response lagged the GWMF by two MJO phases (i.e., 1/2π phase lag), and was prominently positive during MJO P6. The results indicated that the MJO modulation on the zonal GWMFs and zonal winds interacted as a "force–response" system, similar to the roles of GW in the QBO and SAO. In addition, the time-lagged composites revealed that a significant westward GWMF occurred lagging MJO P4 by ∼25–35 days, in agreement with the MJO modulation on the stratospheric polar vortex. The analysis provides a possible explanation for how MJO activity influences GWMFs around the extratropical mesopause, that is, through poleward planetary waves then changing the stratospheric background winds and GW propagation.

Data Availability Statement

Mohe Meteor radar data were provided by Heilongjiang Mohe National Observatory of Geophysics, Institute of Geology and Geophysics, Chinese Academy of Sciences through the National Space Science Data Center (http://wdc.geophys.ac.cn/dbList.asp?dType=MetPublish&dStation=Mohe) (WDC for Geophysics, Beijing, 2024). The MJO RMM index is available at https://psl.noaa.gov/mjo/mjoindex/ (Wheeler & Hendon, 2004). NOAA Interpolated OLR data provided by the NOAA/OAR/ESRL PSD, Boulder, Colorado, USA. ERA-5 data are available for the public from the European Centre for Medium-Range Weather Forecasts at the website https://cds.climate.copernicus.eu/ (ECMWF, 2024).

Acknowledgments

This work was supported by the Project of Stable Support for Youth Team in Basic Research Field, CAS (YSBR-018), the B-type Strategic Priority Program of the Chinese Academy of Sciences (Grant XDB0780000), the National Natural Science Foundation of China (42425403, 42204165, 42394123, 42205067), and the Chinese Meridian Project. We thank all reviewers for their valuable comments and suggestions.

References

Alexander, M. J., Grimsdell, A. W., Stephan, C. C., & Hoffmann, L. (2018). MJO-related intraseasonal variation in the stratosphere: Gravity waves and zonal winds. *Journal of Geophysical Research: Atmospheres*, *123*(2), 775–788. https://doi.org/10.1002/2017JD027620

Andrioli, V. F., Fritts, D. C., Batista, P. P., & Clemesha, B. R. (2013). Improved analysis of all-sky meteor radar measurements of gravity wave variances and momentum fluxes. *Annales Geophysicae*, *31*(5), 889–908. https://doi.org/10.5194/angeo-31-889-2013

Baldwin, M. P., Gray, L. J., Dunkerton, T. J., Hamilton, K., Haynes, P. H., Randel, W. J., et al. (2001). The quasi-biennial oscillation. *Reviews of Geophysics*, *39*(2), 179–229. https://doi.org/10.1029/1999RG000073

Barrett, B. S., Densmore, C. R., Ray, P., & Sanabia, E. R. (2021). Active and weakening mjo events in the maritime continent. *Climate Dynamics*, *57*(1–2), 157–172. https://doi.org/10.1007/s00382-021-05699-8

Becker, E. (2004). Direct heating rates associated with gravity wave saturation. *Journal of Atmospheric and Solar-Terrestrial Physics*, *66*(6–9), 683–696. https://doi.org/10.1016/j.jastp.2004.01.019

Becker, E., & Fritts, D. C. (2006). Enhanced gravity-wave activity and interhemispheric coupling during the MaCWAVE/MIDAS northern summer program 2002. *Annales Geophysicae*, *24*(4), 1175–1188. https://doi.org/10.5194/angeo-24-1175-2006

Cassou, C. (2008). Intraseasonal interaction between the Madden-Julian oscillation and the North Atlantic oscillation. *Nature*, *455*(7212), 523–527. https://doi.org/10.1038/nature07286

Charlton, A. J., & Polvani, L. M. (2007). A new look at stratospheric sudden warmings. Part I: Climatology and modeling benchmarks. *Journal of Climate*, *20*(3), 449–469. https://doi.org/10.1175/JCLI3996.1

Cullens, C. Y., England, S. L., & Garcia, R. R. (2016). The 11 year solar cycle signature on wave-driven dynamics in WACCM. *Journal of Geophysical Research: Space Physics*, *121*(4), 3484–3496. https://doi.org/10.1002/2016JA022455

de Wit, R. J., Janches, D., Fritts, D. C., & Hibbins, R. E. (2016). QBO modulation of the mesopause gravity wave momentum flux over Tierra del Fuego. *Geophysical Research Letters*, *43*(8), 4049–4055. https://doi.org/10.1002/2016GL068599

Domeisen, D. I., Garfinkel, C. I., & Butler, A. H. (2019). The teleconnection of El Niño southern oscillation to the stratosphere. *Reviews of Geophysics*, *57*(1), 5–47. https://doi.org/10.1029/2018RG000596

Eckermann, S. D., Rajopadhyaya, D. K., & Vincent, R. A. (1997). Intraseasonal wind variability in the equatorial mesosphere and lower thermosphere: Long-term observations from the central Pacific. *Journal of Atmospheric and Solar-Terrestrial Physics*, *59*(6), 603–627. https://doi.org/10.1016/S1364-6826(96)00143-5

Eckermann, S. D., & Vincent, R. A. (1994). First observations of intraseasonal oscillations in the equatorial mesosphere and lower thermosphere. *Geophysical Research Letters*, *21*(4), 265–268. https://doi.org/10.1029/93GL02835

ECMWF. (2024). ERA5 hourly data on pressure levels from 1959 to present [Dataset]. https://cds.climate.copernicus.eu/

Ern, M., Diallo, M., Preusse, P., Mlynczak, M. G., Schwartz, M. J., Wu, Q., & Riese, M. (2021). The semiannual oscillation (SAO) in the tropical middle atmosphere and its gravity wave driving in reanalyses and satellite observations. *Atmospheric Chemistry and Physics*, *21*(18), 13763–13795. https://doi.org/10.5194/acp-21-13763-2021

Ern, M., Ploeger, F., Preusse, P., Gille, J. C., Gray, L. J., Kalisch, S., et al. (2014). Interaction of gravity waves with the QBO: A satellite perspective. *Journal of Geophysical Research: Atmospheres*, *119*(5), 2329–2355. https://doi.org/10.1002/2013JD020731

Fritts, D. C., & Alexander, M. J. (2003). Gravity wave dynamics and effects in the middle atmosphere. *Reviews of Geophysics*, *41*(1). https://doi.org/10.1029/2001RG000106

Fritts, D. C., Janches, D., & Hocking, W. K. (2010). Southern Argentina Agile Meteor Radar: Initial assessment of gravity wave momentum fluxes. *Journal of Geophysical Research*, *115*(D19). https://doi.org/10.1029/2010JD013891

Garfinkel, C. I., Benedict, J. J., & Maloney, E. D. (2014). Impact of the MJO on the boreal winter extratropical circulation. *Geophysical Research Letters*, *41*(16), 6055–6062. https://doi.org/10.1002/2014GL061094

Garfinkel, C. I., Feldstein, S. B., Waugh, D. W., Yoo, C., & Lee, S. (2012). Observed connection between stratospheric sudden warming and the Madden-Julian Oscillation. *Geophysical Research Letters*, *39*(18). https://doi.org/10.1029/2012GL053144

Gasperini, F., Liu, H., & McInerney, J. (2020). Preliminary evidence of Madden-Julian Oscillation effects on ultrafast tropical waves in the thermosphere. *Journal of Geophysical Research: Space Physics*, *125*(5), e2019JA027649. https://doi.org/10.1029/2019ja027649

Gong, Y., Xue, J., Ma, Z., Zhang, S., Zhou, Q., Huang, C., et al. (2022). Observations of a strong intraseasonal oscillation in the MLT region during the 2015/2016 winter over Mohe, China. *Journal of Geophysical Research: Space Physics*, *127*(6), e2021JA030076. https://doi.org/10.1029/2021JA030076

Gupta, A., Birner, T., Dörnbrack, A., & Polichtchouk, I. (2021). Importance of gravity wave forcing for springtime southern polar vortex breakdown as revealed by ERA5. *Geophysical Research Letters*, *48*(10), e2021GL092762. https://doi.org/10.1029/2021GL092762

Hersbach, H., Bell, B., Berrisford, P., Hirahara, S., Horányi, A., Muñoz-Sabater, J., et al. (2020). The ERA5 global reanalysis. *Quarterly Journal of the Royal Meteorological Society*, *146*(730), 1999–2049. https://doi.org/10.1002/qj.3803

Hocking, W. K. (2005). A new approach to momentum flux determinations using SKiYMET meteor radars. *Annales Geophysicae*, *23*(7), 2433–2439. https://doi.org/10.5194/angeo-23-2433-2005

Hsiao, W.-T., Maloney, E. D., & Barnes, E. A. (2020). Investigating recent changes in MJO precipitation and circulation in multiple reanalyses. *Geophysical Research Letters*, *47*(22), e2020GL090139. https://doi.org/10.1029/2020GL090139

Jia, M., Xue, X., Gu, S., Chen, T., Ning, B., Wu, J., et al. (2018). Multiyear observations of gravity wave momentum fluxes in the midlatitude mesosphere and lower thermosphere region by meteor radar. *Journal of Geophysical Research: Space Physics*, *123*(7), 5684–5703. https://doi.org/10.1029/2018JA025285

Kang, W., & Tziperman, E. (2017). More frequent sudden stratospheric warming events due to enhanced MJO forcing expected in a warmer climate. *Journal of Climate*, *30*(21), 8727–8743. https://doi.org/10.1175/JCLI-D-17-0044.1

Kang, W., & Tziperman, E. (2018). The MJO-SSW teleconnection: Interaction between MJO-forced waves and the midlatitude jet. *Geophysical Research Letters*, *45*(9), 4400–4409. https://doi.org/10.1029/2018GL077937

Karlsson, B., Körnich, H., & Gumbel, J. (2008). Evidence for interhemispheric stratosphere-mesosphere coupling derived from noctilucent cloud properties. *Geophysical Research Letters*, *34*(16). https://doi.org/10.1029/2007GL030282

Karlsson, B., Randall, C. E., Benze, S., Mills, M., Russell, J. M., & Bailey, S. M. (2009). Intra-seasonal variability of polar mesospheric clouds due to inter-hemispheric coupling. *Geophysical Research Letters*, *36*(20). https://doi.org/10.1029/2009GL040348

Kumari, K., Oberheide, J., & Lu, X. (2020). The tidal response in the mesosphere/lower thermosphere to the Madden-Julian oscillation observed by SABER. *Geophysical Research Letters*, *47*(16), e2020GL089172. https://doi.org/10.1029/2020gl089172

Kumari, K., Wu, H., Long, A., Lu, X., & Oberheide, J. (2021). Mechanism studies of Madden-Julian Oscillation coupling into the mesosphere/lower thermosphere tides using SABER, MERRA-2, and SD-WACCMX. *Journal of Geophysical Research: Atmospheres*, *126*(13), e2021JD034595. https://doi.org/10.1029/2021JD034595

Li, J., & Lu, X. (2020). SABER observations of gravity wave responses to the Madden-Julian Oscillation from the stratosphere to the lower thermosphere in tropics and extratropics. *Geophysical Research Letters*, *47*(23), e2020GL091014. https://doi.org/10.1029/2020GL091014

Li, J., & Lu, X. (2021). Global responses of gravity waves and zonal mean winds to the Madden-Julian Oscillation and the latitudinal dependence of their relations using MERRA-2. *Geophysical Research Letters*, *48*(20), e2021GL094717. https://doi.org/10.1029/2021GL094717

Li, T., Calvo, N., Yue, J., Russell, J. M., III, Smith, A. K., Mlynczak, M. G., et al. (2016). Southern hemisphere summer mesopause responses to El Niño–southern oscillation. *Journal of Climate*, *29*(17), 6319–6328. https://doi.org/10.1175/JCLI-D-15-0816.1

Li, Z., Chu, X., Harvey, V. L., Jandreau, J., Lu, X., Yu, Z., et al. (2020). First lidar observations of quasi-biennial oscillation-induced interannual variations of gravity wave potential energy density at McMurdo via a modulation of the Antarctic polar vortex. *Journal of Geophysical Research: Atmospheres*, *125*(16), e2020JD032866. https://doi.org/10.1029/2020JD032866

Lin, H., Brunet, G., & Derome, J. (2009). An observed connection between the North Atlantic oscillation and the Madden–Julian oscillation. *Journal of Climate*, *22*(2), 364–380. https://doi.org/10.1175/2008JCLI2515.1

Liu, A. Z., Lu, X., & Franke, S. J. (2013). Diurnal variation of gravity wave momentum flux and its forcing on the diurnal tide. *Journal of Geophysical Research: Atmospheres*, *118*(4), 1668–1678. https://doi.org/10.1029/2012JD018653

Liu, C., Tian, B., Li, K.-F., Manney, G. L., Livesey, N. J., Yung, Y. L., & Waliser, D. E. (2014). Northern hemisphere mid-winter vortex-displacement and vortex-split stratospheric sudden warming: Influence of the Madden-Julian oscillation and quasi-biennial oscillation. *Journal of Geophysical Research: Atmospheres*, *119*(22), 12–599. https://doi.org/10.1002/2014JD021876

Liu, G., Janches, D., & Lieberman, R. S. (2018). Intraseasonal variations of nonmigrating tides observed near the mesopause. *Journal of Geophysical Research: Space Physics*, *123*(11), 9921–9931. https://doi.org/10.1029/2018JA025709

Liu, X., Xu, J., Yue, J., & Kogure, M. (2022). Strong gravity waves associated with Tonga volcano eruption revealed by SABER observations. *Geophysical Research Letters*, *49*(10), e2022GL098339. https://doi.org/10.1029/2022GL098339

Madden, R. A., & Julian, P. R. (1971). Detection of a 40–50 day oscillation in the zonal wind in the tropical Pacific. *Journal of the Atmospheric Sciences*, *28*(5), 702–708. https://doi.org/10.1175/1520-0469(1971)028<0702:DOADOI>2.0.CO;2

Madden, R. A., & Julian, P. R. (1972). Description of global-scale circulation cells in the tropics with a 40–50 day period. *Journal of the Atmospheric Sciences*, *29*(6), 1109–1123. https://doi.org/10.1175/1520-0469(1972)029<1109:DOGSCC>2.0.CO;2

Moss, A. C., Wright, C. J., & Mitchell, N. J. (2016). Does the Madden-Julian Oscillation modulate stratospheric gravity waves? *Geophysical Research Letters*, *43*(8), 3973–3981. https://doi.org/10.1002/2016GL068498

Placke, M., Stober, G., & Jacobi, C. (2011). Gravity wave momentum fluxes in the MLT—Part I: Seasonal variation at Collm (51.3°N, 13.0°E). *Journal of Atmospheric and Solar-Terrestrial Physics*, *73*(9), 904–910. https://doi.org/10.1016/j.jastp.2010.07.012

Pramitha, M., Kumar, K. K., Ratnam, M. V., Praveen, M., & Rao, S. V. B. (2020). Gravity wave source spectra appropriation for mesosphere lower thermosphere using meteor radar observations and GROGRAT model simulations. *Geophysical Research Letters*, *47*(19), e2020GL089390. https://doi.org/10.1029/2020GL089390

Ren, P., Kim, D., Ahn, M., Kang, D., & Ren, H. (2021). Intercomparison of MJO column moist static energy and water vapor budget among six modern reanalysis products. *Journal of Climate*, *34*(8), 2977–3001. https://doi.org/10.1175/JCLI-D-20-0653.1

Salminen, A., Asikainen, T., Maliniemi, V., & Mursula, K. (2020). Dependence of sudden stratospheric warming on internal and external drivers. *Geophysical Research Letters*, *47*(5), e2019GL086444. https://doi.org/10.1029/2019GL086444

Schwartz, C., & Garfinkel, C. I. (2020). Troposphere-stratosphere coupling in subseasonal-to-seasonal models and its importance for a realistic extratropical response to the Madden-Julian Oscillation. *Journal of Geophysical Research: Atmospheres*, *125*(10), e2019JD032043. https://doi.org/10.1029/2019JD032043

Song, B., Chun, H., & Song, I. (2020). Role of gravity waves in a vortex-split sudden stratospheric warming in January 2009. *Journal of the Atmospheric Sciences*, *77*(10), 3321–3342. https://doi.org/10.1175/JAS-D-20-0039.1

Sun, C., Yang, C., & Li, T. (2021). Dynamical influence of the Madden-Julian oscillation on the Northern Hemisphere mesosphere during the boreal winter. *Science China Earth Sciences*, *64*(8), 1254–1266. https://doi.org/10.1007/s11430-020-9779-2

Thurairajah, B., Bailey, S. M., Cullens, C. Y., Hervig, M. E., & Russell, J. M. (2014). Gravity wave activity during recent stratospheric sudden warming events from SOFIE temperature measurements. *Journal of Geophysical Research: Atmospheres*, *119*(13), 8091–8103. https://doi.org/10.1002/2014JD021763

Triplett, C. C., Li, J., Collins, R. L., Lehmacher, G. A., Barjatya, A., Fritts, D. C., et al. (2018). Observations of reduced turbulence and wave activity in the Arctic middle atmosphere following the January 2015 sudden stratospheric warming. *Journal of Geophysical Research: Atmospheres*, *123*(23), 13259–13276. https://doi.org/10.1029/2018JD028788

Tsuchiya, C., Sato, K., Alexander, M. J., & Hoffmann, L. (2016). MJO-related intraseasonal variation of gravity waves in the Southern Hemisphere tropical stratosphere revealed by high-resolution AIRS observations. *Journal of Geophysical Research: Atmospheres*, *121*(13), 7641–7651. https://doi.org/10.1002/2015JD024463

Vadas, S. L., Liu, H. L., & Lieberman, R. S. (2014). Numerical modeling of the global changes to the thermosphere and ionosphere from the dissipation of gravity waves from deep convection. *Journal of Geophysical Research: Space Physics*, *119*(9), 7762–7793. https://doi.org/10.1002/2014JA020280

Vincent, R. A., Kovalam, S., Reid, I. M., & Younger, J. P. (2010). Gravity wave flux retrievals using meteor radars. *Geophysical Research Letters*, *37*(14). https://doi.org/10.1029/2010GL044086

Vitart, F., & Molteni, F. (2010). Simulation of the Madden– Julian oscillation and its teleconnections in the ECMWF forecast system. *Quarterly Journal of the Royal Meteorological Society*, *136*(649), 842–855. https://doi.org/10.1002/qj.623

Wang, F., Tian, W., Xie, F., Zhang, J., & Han, Y. (2018). Effect of Madden–Julian Oscillation occurrence frequency on the interannual variability of northern hemisphere stratospheric wave activity in winter. *Journal of Climate*, *31*(13), 5031–5049. https://doi.org/10.1175/JCLI-D-17-0476.1

WDC for Geophysics, Beijing. (2024). Daily MET data of Mohe meteor radar [Dataset]. http://wdc.geophys.ac.cn/dbList.asp?dType=MetPublish&dStation=Mohe

Wheeler, M. C., & Hendon, H. H. (2004). An all-season real-time multivariate mjo index: Development of an index for monitoring and prediction. *Monthly Weather Review*, *132*(8), 1917–1932. https://doi.org/10.1175/1520-0493(2004)132<1917:AARMMI>2.0.CO;2

Yadav, P., Garfinkel, C. I., & Domeisen, D. I. V. (2024). The role of the stratosphere in teleconnections arising from fast and slow MJO episodes. *Geophysical Research Letters*, *51*(1), e2023GL104826. https://doi.org/10.1029/2023GL104826

Yamazaki, Y. (2023). A method to derive Fourier–wavelet spectra for the characterization of global-scale waves in the mesosphere and lower thermosphere and its MATLAB and Python software (fourierwavelet v1.1). *Geoscientific Model Development*, *16*(16), 4749–4766. https://doi.org/10.5194/gmd-16-4749-2023

Yang, C., Li, T., Xue, X., Gu, S.-Y., Yu, C., & Dou, X. (2019). Response of the northern stratosphere to the Madden-Julian oscillation during boreal winter. *Journal of Geophysical Research: Atmospheres*, *124*(10), 5314–5331. https://doi.org/10.1029/2018JD029883

Yang, C., Smith, A. K., Li, T., & Dou, X. (2018). The effect of the Madden-Julian oscillation on the mesospheric migrating diurnal tide: A study using SD-WACCM. *Geophysical Research Letters*, *45*(10), 5105–5114. https://doi.org/10.1029/2018GL077956

Zhang, C. (2005). Madden-Julian oscillation. *Reviews of Geophysics*, *43*(2). https://doi.org/10.1029/2004rg000158

Zhou, W., Yang, D., Xie, S.-P., & Ma, J. (2020). Amplified Madden–Julian oscillation impacts in the Pacific–North America region. *Nature Climate Change*, *10*(7), 654–660. https://doi.org/10.1038/s41558-020-0814-0

Zhou, X., Yue, X., Chen, G., Yu, Y., & Hu, L. (2023). MJO modulation on the intraseasonal variability of MLT DE3 tide in winds. *Chinese Journal of Geophysics*, *66*(12), 4817–4827. https://doi.org/10.6038/cjg2023R0311

Zhou, X., Yue, X., Liu, L., Yu, Y., Ding, F., Ren, Z., et al. (2022). Decadal continuous meteor-radar estimation of the mesopause gravity wave momentum fluxes over Mohe: Capability evaluation and interannual variation. *Remote Sensing*, *14*(22), 5729. https://doi.org/10.3390/rs14225729